Available online at www.sciencedirect.com

ScienceDirect

Ceramics International 40 (2014) 4055–4064

CERAMICS INTERNATIONAL

www.elsevier.com/locate/ceramint

Growth and optical properties of cerium dioxide nanocrystallites prepared by coprecipitation routes

Horng-Huey Ko[a], Guoli Yang[b,c], Huy-Zu Cheng[d], Moo-Chin Wang[a,*], XiuJian Zhao[b,**]

[a]Department of Fragrance and Cosmetic Science, Kaohsiung Medical University, 100 Shih-Chuan 1st Road, Kaohsiung 80708, Taiwan
[b]State Key Laboratory of Silicate Materials for Architectures (Wuhan University of Technology), Wuhan 430070, People's Republic of China
[c]Teaching and Research Section for Mechanical Foundation, Foundation Department, Wuhan 430070, PR China
[d]Department of Materials Science and Engineering, I-Shou University, 1 Huseh-Cheng Road, Section 1, Ta-Hsu, Kaohsiung 84001, Taiwan

Received 12 June 2013; received in revised form 24 July 2013; accepted 12 August 2013
Available online 20 August 2013

Abstract

Nanosized cerium dioxide (CeO_2) powders have been synthesized using coprecipitation methods and cerium nitrate hexahydrate ($Ce(NO_3)_3 \cdot 6H_2O$) as the starting material. The growth and optical properties of nanosized CeO_2 powders were investigated using X-ray diffraction (XRD), transmission electron microscopy (TEM), selected area electron diffraction (SAED), nano-beam electron diffraction (NBED), high resolution TEM (HRTEM), and ultraviolet–visible (UV–vis) absorption spectrophotometry. The XRD result shows that the dried CeO_2 precursor powders (both before and after calcination at various temperatures and times) contained a single crystalline phase of CeO_2. In the dried precursor powders, the crystallites of CeO_2 measured 10.4 nm and 66.8 nm before and after calcination at 1273 K for 240 min, respectively. The indirect band gap energy (E_i) of CeO_2 decreased from 3.03 eV to 2.68 eV as the crystallite size increased from 10.4 nm to 66.8 nm, whereas the direct band gap energy (E_d) of CeO_2 also decreased from 3.79 eV to 3.38 eV.

Keywords: C. Optical properties; D. CeO_2; Crystallite size; Band gap energy

1. Introduction

Materials based on cerium dioxide (CeO_2) are important due to their extensive use in applications, such as gas sensors [1], solid oxide fuel cells [2,3], auto exhaust emission control [4,5], catalytic wet oxidation [5], photocatalytic oxidation of water [6], glass polishing materials [7], ultraviolet (UV) absorbents and filters [8], optical, electro-optical, microelectronic and opto-electronic devices [9]. Recently, nanosized particles have attracted considerable attention because their physical and chemical properties are significantly different from those of the bulk materials [10]. CeO_2 nanocrystallite powders have considerable potential for use as UV absorbents and high-activity catalysts.

When using CeO_2 for UV absorbents and filters applications, the crystallite size and morphology significantly influence the absorption properties. Recently, numerous routes for synthesizing nanosized CeO_2 particles with promising control of properties have been reported, such as hydrothermal [11], sonochemical [12], sol–gel [13], microwave [14], microemulsion [15], reverse micelles [16], and homogeneous precipitation. Among these routes, homogeneous precipitation is one of the most promising techniques because of its low cost, easy-to-acquire apparatus, simple synthesis process, and nanometric precursor particles.

The synthesis of CeO_2 rhombic microplates prepared at room temperature via ultrasonication using polyethylene glycol as a structure-directing agent has been reported by Zhang et al. [17]. The authors noted that polycrystalline CeO_2 nanorods with 5–10 nm diameters and 50–150 nm lengths were obtained. In addition, Hassananzadeh-Tabrizi et al. [18] proposed that the activation energy of CeO_2 nanopowder growth is 14.6 kJ/mol for the precursors obtained using the reverse precipitation synthesis process. The activation energy of 56.42 kJ/mol has been reported

*Corresponding author. Tel.: +886 7 3121101x2366.
**Corresponding author. Tel.: +86 13871110463.
E-mail addresses: mcwang@kmu.edu.tw (M.-C. Wang), opluse@whut.edu.cn (X. Zhao).

0272-8842/$ - see front matter © 2013 Elsevier Ltd and Techna Group S.r.l. All rights reserved.
http://dx.doi.org/10.1016/j.ceramint.2013.08.059

by Yang et al. for CeO_2 growth from precursor powders obtained via coprecipitation routes [19]. Conversely, Liu et al. [20] used a facile one-step hydrothermal process to prepare CeO_2 nanosheets with a (110) dominated surface that exhibits an obvious blue-shift in UV absorbance compared to bulk CeO_2. Moreover, Lu et al. [21] noted that the absorption edge for octahedrons and spheres red-shifted and that the absorption edge of the octahedrons was near the visible region.

Although the precipitation technique has been widely used for CeO_2 nanoparticle synthesis, most studies were focused on the effects of the cerium precursors, ligands, additives, and reaction media on CeO_2 nanocrystallite formation. However, the growth and optical properties of nanosized CeO_2 crystallites have not been studied in detail. In this study, the crystallite growth and optical properties of CeO_2 precursor powders prepared from cerium nitrate via coprecipitation routes were investigated in detail. Characteristics of the CeO_2 powders were determined using X-ray diffraction (XRD), transmission electron microscopy (TEM), selected area electron diffraction (SAED), nano-beam electron diffraction (NBED), high resolution TEM (HRTEM) and UV–vis spectrophotometry.

The purposes of this investigation were (i) to study the growth behavior of CeO_2 powders of the dried precursor powders after calcination, (ii) to study the effect of crystallite size on the optical properties of CeO_2 powders, and (iii) to examine the TEM microstructure of uncalcined and calcined CeO_2 powders.

2. Experimental procedures

2.1. Sample preparation

In this study, cerium nitrate hexahydrate ($Ce(NO_3)_3 \cdot 6H_2O$, purity $\geq 99.0\%$, supplied by Sinopharm Chemical Reagent Co., Ltd., China) was used as the starting material. Polyethylene glycol (PEG, MW 600, supplied by Sinopharm Chemical Reagent Co., Ltd., China) was used as a dispersant. Cerium nitrate hexahydrate was dissolved in a solution of deionized water and ethanol at a volume ratio of 4:1. A concentration of $Ce(NO_3)_3$ equal to 0.1 mol/L in solution was prepared, and 1 wt% PEG was added as a dispersion agent for reducing agglomeration. The mixed solution was stirred by a magnetic stirrer at 293 K. Next, NH_4OH (supplied by Sinopharm Chemical Reagent Co., Ltd., China) was slowly added into the solution until a pH value of 9 was obtained. After precipitation, the precipitates were repeatedly rinsed with a large amount of deionized water and ethanol. Subsequently, the precursor powders were dried at 313 K in an oven. Finally, the cerium dioxide dried precursor powders after calcination at various temperatures and durations.

2.2. Sample characterization

The crystalline phase was identified using X-ray diffraction (XRD, Rigaku D/MAX-RB X-ray, Tokyo) with Cu Kα radiation and a Ni filter operating at 40 kV, 50 mA, and a scanning rate (2θ) of 1°/min. The average crystallite size of the dried cerium oxide precursor powders after calcination at different temperatures for various durations was determined using Scherrer's equation [22] as follows:

$$D_{hkl} = \frac{0.89\lambda}{\beta \cos \theta} \quad (1)$$

where D_{hkl} denotes the average crystallite size of the CeO_2 powders, $\lambda = 0.15405$ nm is the X-ray wavelength of Cu Kα, β is the full-width at half maximum intensity (FWHM) of the peak, and θ is the Bragg's angle of the peak.

The ultraviolet–visible (UV–vis) (UV-3600, Shimadzu Co., Japan) diffuse reflectance spectra were performed under ambient conditions with an integrating sphere. $BaSO_4$ was used as a reference, and spectra were recorded over the range of 200–600 nm.

The UV–vis absorption spectra of the dried cerium oxide precursor powders and the products of calcination dispersed in water were recorded for the determination of the band gap energies. The optical absorption coefficient, α, was calculated using the following equation [11,23–25]:

$$\alpha = \frac{2.303 \times 10^3 A\beta}{lc} \quad (2)$$

where A is the absorbance of the product sample, β is the real density of CeO_2 (7.172 g/cm^3), l is the path length of the quartz cell (1.0 cm), and c is the concentration of the product sample in the suspensions.

The morphology of the dried cerium oxide precursor powders before and after calcination was examined using transmission electron microscopy (TEM, JEM-2010 Electron Microscope, JEOL Co., Tokyo, Japan) operating at 200 kV. The TEM sample was prepared by dispersing the CeO_2 powders in an ultrasonic bath and then collecting on a copper grid. SAED and NBED examinations were also made on the TEM sample.

3. Results and discussion

3.1. The growth behavior of the cerium dioxide dried precursor powders after calcination

XRD patterns of the dried cerium dioxide precursor powders after calcination at various temperatures for 240 min are presented in Fig. 1. The XRD pattern reveals reflection peaks of (1 1 1), (2 0 0), (2 2 0), and (3 1 1) for the dried precursor powders before calcination as dried precursor powders, which correspond to cerium dioxide (CeO_2). This phenomenon is attributed to crystalline CeO_2 in the dried cerium oxide precursor powders. However, the broad and weak intensity of the dried CeO_2 precursor powder peaks showed poor crystallinity and/or a composition of finer crystallites in the nanometer to submicron range [26,27]. When the calcination temperature was increased to 673 K, the XRD pattern still exhibited broad and weak peaks that were nearly unchanged. This result occurred because the CeO_2 powders maintained poor crystallinity and finer crystallite size when the calcination

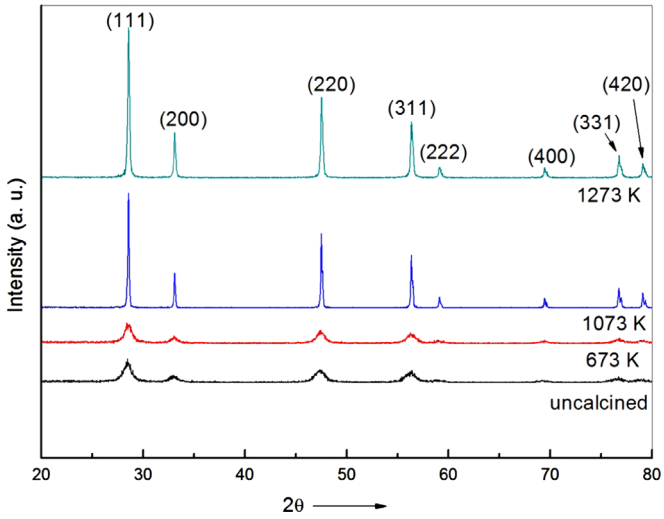

Fig. 1. XRD patterns of CeO_2 dried precursor powders after calcination at various temperatures for 240 min.

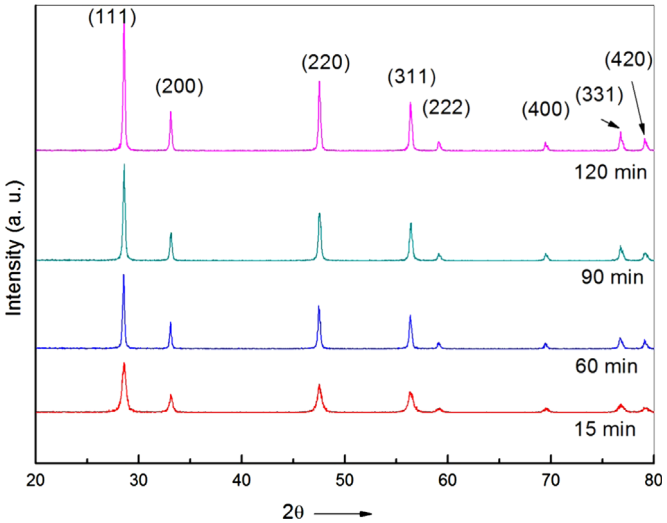

Fig. 2. XRD patterns of CeO_2 dried precursor powders after calcination at 1073 K for various times.

temperature was below 673 K; however, the reflection peaks became sharper and stronger when the dried precursor powders after calcination at 1073 K and 1273 K. This result occurred because the crystallite size increased and crystallinity improved for CeO_2 powders as the calcination temperature increased.

Fig. 2 shows the XRD patterns of the cerium oxide dried precursor powders after calcination at 1073 K for various times. The XRD pattern of dried precursor powders after calcination at 1073 K for 15 min shows broad and weak peaks, which is attributed to the CeO_2 powders maintaining poor crystallinity and fine crystallite [28,29]. When the duration increased to 60 min, the peaks became obviously sharp. As the duration further increased to 120 min, the intensity of the reflections only increased slowly. These results reveal that the crystallite size and crystallinity growth of CeO_2 rapidly increased with increasing time from 15 min to 60 min, then the rate of crystallite growth only increased slowly.

Fig. 3 shows the crystallite size of the dried cerium dioxide precursor powders after calcination at various temperatures for 240 min, which reveals that the crystallite size remained almost unchanged for calcination temperatures below 673 K, whereas the crystallite size of CeO_2 obviously increased when the calcination temperature was greater than 873 K. The crystallite size of CeO_2 has an exponential dependence on the calcination temperature because the growth of the CeO_2 crystallite was diffusion controlled [19,28]. Moreover, Lai et al. [29] also noted that the relationship between crystallite size and calcination temperature has an exponential dependence because the impurities usually exist in the interface regions and slow the crystallite growth front for nanostructure ceramics.

The crystallite size of the dried CeO_2 precursor powders after calcination at various temperatures for 240 min was determined using XRD line broadening of the reflection. The crystallite size of CeO_2 remained almost unchanged when the calcination temperature was below 673 K. In contrast, the

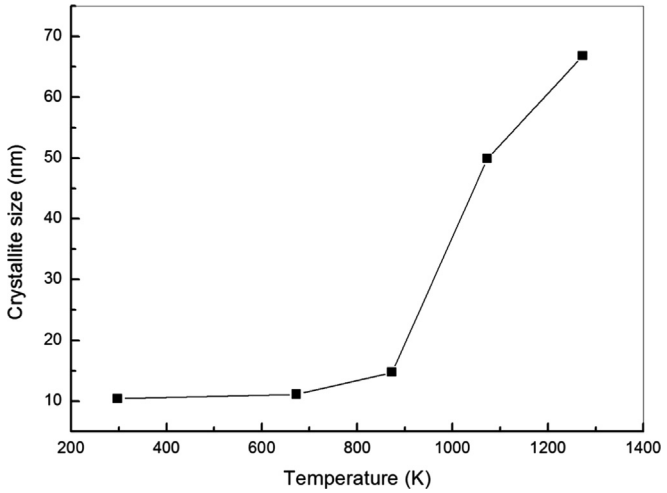

Fig. 3. The average crystallite sizes of the dried cerium dioxide precursor powders before and after calcination at various temperatures for 240 min.

crystallite size underwent an obvious increase when the calcinations temperature was greater than 873 K. Li et al. [21] noted that the crystallite size of CeO_2 showed an exponential dependence on the calcination temperature because the growth of CeO_2 crystallites was controlled by the diffusion.

Fig. 4 shows the crystallite sizes of the CeO_2 dried precursor powders after calcination at various temperatures for various durations. It reveals that the crystallite size only increased slightly from 10.4 to 11.2 nm (only an increment of 7.7%) after calcination at 673 K for 5 to 240 min. In addition, the crystallite size rapidly grew from 18.1 nm to 46.4 nm when the dried precursor powders after calcination at 1073 K from 5 to 120 min. The crystallite sizes were 43.0 nm and 54.8 nm when the crystallite sizes of the dried CeO_2 precursor powders after calcination at 1273 K for 5 min and 15 min, respectively. Next, the crystallite size only grew slowly (from 57.2 nm to 66.8 nm) as they calcined at 1273 K from 30 min to 120 min.

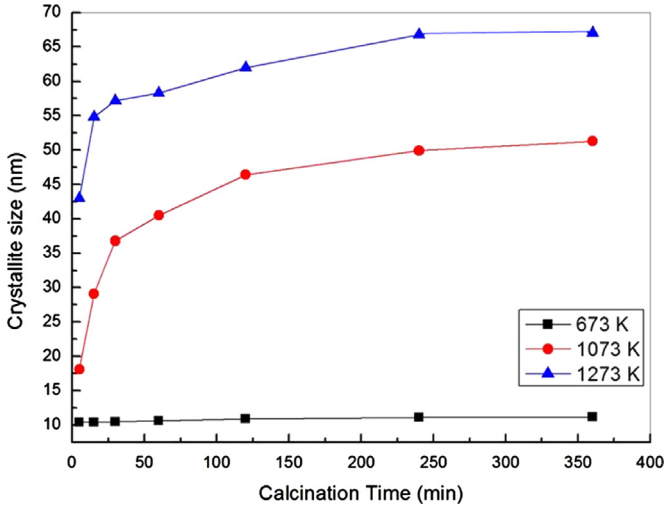

Fig. 4. The average crystallite sizes of the dried cerium dioxide precursor powders after calcination at various temperatures and durations.

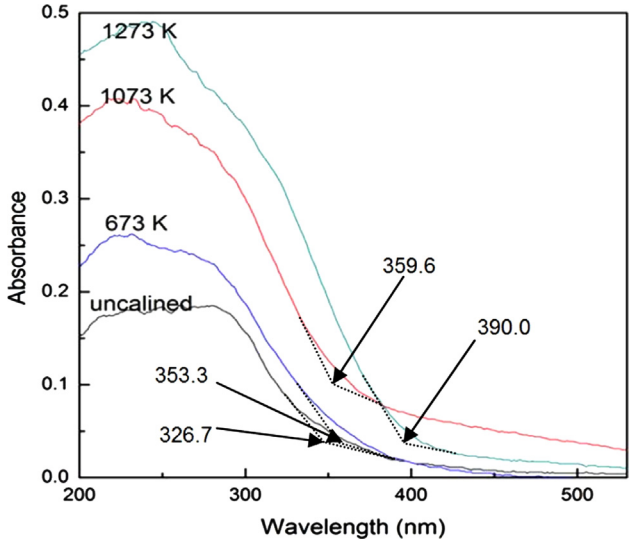

Fig. 5. The UV–vis absorption spectra of cerium dioxide precursor powders after calcination at different temperatures for 240 min.

In contrast, the crystallite size increased rapidly as the duration increased from 5 to 60 min when the calcination temperature was greater than 1073 K. This result suggests that the pores in the interior of the dried precursor powders were rapidly eliminated under these conditions.

3.2. The effect of crystallite size on the optical properties

The UV–vis absorption spectra of the cerium dioxide dried precursor powders before and after calcination at various temperatures for 240 min are shown in Fig. 5. All the samples exhibited a strong and distinct absorption band between 270 and 340 nm in the UV region due to the charge-transfer transitions from O 2p to Ce 4f, which swamped the well-known f–f spin orbit splitting of the Ce 4f state [30,31]. No absorptions were detected for wavelengths longer than 500 nm. In addition, Fig. 5 also shows that the edge absorption obtained by tangent method which shows red-shifted a small amount from 326.7 nm in the dried precursor powders to 390.0 nm for dried precursor powders after calcination at 1273 K for 240 min. Moreover, the absorption intensity increased with increasing calcination temperature. This result was observed because the higher calcination temperature causes the particle size to increase, leading to intense absorption.

de Lima et al. [32] have studied the ultrafine systems of ZnO:CeO_2=9:1 for use as ultraviolet filter. They pointed out that the synthesized samples display low reflectance in the all region of 280–320 nm, which means high absorption. In the range of 320–400 nm, the synthesized samples display high absorption from 320 to 350 nm, and the reflectance starts to increase at 350 nm for compounds. However, this behavior was more pronounced in the ZnO, which present a steeper slope than all the other samples, therefore the synthesized samples were really promising. In addition, TiO_2 fine particles were embedded with sunscreens into the skin to effectively attenuate UV-B radiation also reported by Popov et al. [33]. They pointed out that TiO_2 particles of 62 nm were found to be the most effective in protecting skin against UV-B radiation of 307–311 nm. In the present study, the spectrum of each sample shows that most of the UV light (200–350 nm) was blocked allowing CeO_2 nanopowders to be used as UV blockers.

Knowledge of the wavelength-dependent absorption coefficient allows for the determination of the band gap energy of the dried cerium oxide precursor powders before and after calcination. Electronic transitions occurred from the valance band to the conduction band when the energy of the photon exceeded the band gap energy. These transitions can take place through either a direct or an indirect process [34]. A direct transition is one where only a photon is involved in exciting an electron to the conduction band. An indirect transition is a process which involves a photon and also a phonon that is either emitted or absorbed in the excitation event [34]. To estimate the indirect (E_i) and direct (E_d) band gap energies of dried cerium oxide precursor powders before and after calcination, we calculated $\alpha^{1/2}$ versus photon energy ($h\nu$) and $(\alpha h\nu)^2$ versus photon energy ($h\nu$) for the product samples, respectively.

The indirect band gap energy (E_i) for the CeO_2 nanocrystallites is determined by fitting the absorption data to the following equation [35]:

$$\alpha = B_i(h\nu - E_i)^2 \quad (3)$$

where α is the optical absorption coefficient, $h\nu$ is the photon energy, E_i is the indirect band gap energy and B_i is a constant for indirect transition.

The plot of $\alpha^{1/2}$ vs photon energy (eV) for CeO_2 crystallites is shown in Fig. 6(a). From the intersection of the extrapolated linear portion, the indirect band gap energy (E_i) values of the cerium oxide dried precursor powders was determined, before and after calcination at various temperatures for 240 min, as 3.03, 2.96, 2.78, and 2.68 eV. Fig. 6(a) also shows that the E_i value decreased with increasing the calcination temperature. Moreover, these values also indicated that the E_i value of dried

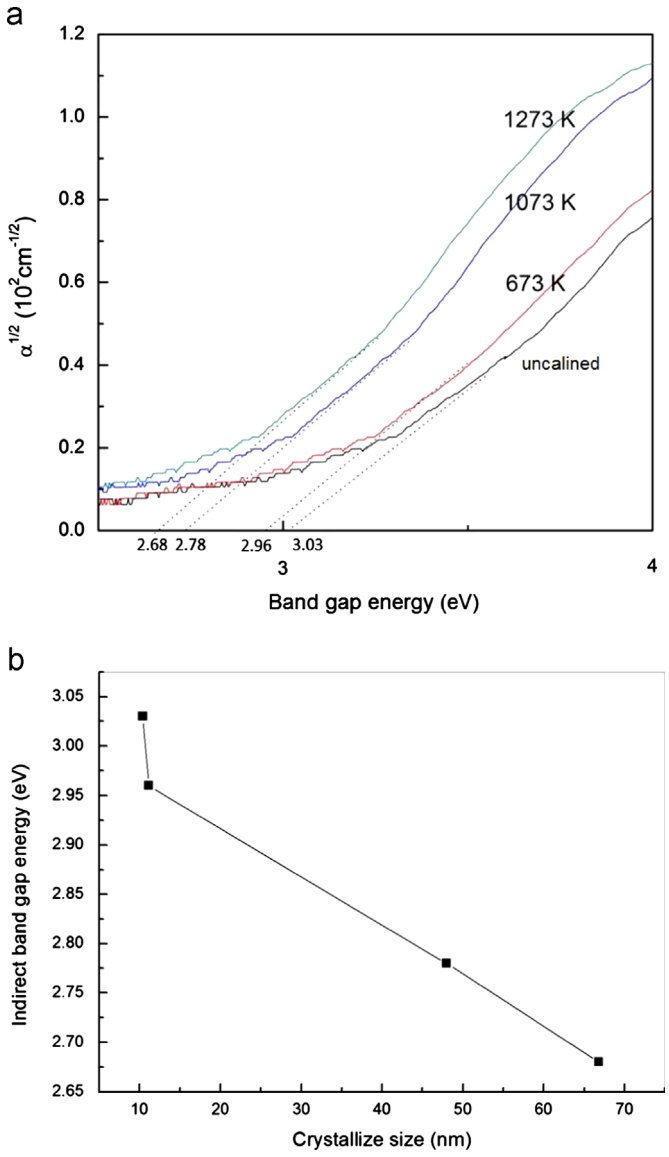

Fig. 6. (a) The dependence of $\alpha^{1/2}$ and photon energy of CeO_2 nanoparticles for the dried precursor powders after different calcination temperatures for 240 min, (b) the relationship between the indirect band gap energy (E_i) and crystallites size of CeO_2 for the dried precursor powders after calcination at various temperatures for 240 min.

cerium precursor powders before calcination was slightly larger than the E_i value of bulk CeO_2 (3.01 eV) [36]. However, other E_i values of samples after calcination were smaller than 3.01 eV. This result revealed that the value of E_i depended on the crystallite size. Therefore, the dependence of the E_i value on the crystallite size of CeO_2 is shown in Fig. 6(b). This trend reveals that the values of E_i decreased from 2.96 eV to 2.68 eV as the crystallite size increased from 11.1 nm to 66.8 nm. These values are within the range reported in the literature. For example, changes in E_i values from 2.88 eV to 2.72 eV have been reported by Taguchi et al. for CeO_2 nanoparticles prepared by displaying one carboxyl group on the surface of the nanocrystals [25]. They also observed the E_i values ranging from 2.82 eV to 3.01 eV for CeO_2 nanoparticles synthesized using a hydrothermal process [11].

A red-shift of the UV absorption spectra of CeO_2 nanostructures has previously been observed [21,36–39]. However, Lu et al. [21] also noted that the true mechanism of the red-shift of CeO_2 nanoparticles is still not clear. In the recent years, two types of mechanisms have been demonstrated to explain the red-shift of the optical band gap of CeO_2 nanostructures: one mechanism is the presence of defects resulting in charge transfer between Ce^{3+} and Ce^{4+} ions, which is the generally accepted mechanism for the red-shift of CeO_2 films [21,34,37,38]. In addition, Patsalas et al. [40] have proposed that the red-shift of the optical band gap of CeO_2 films is correlated with an increase in the Ce^{3+} concentration, and the defects are directly proportional to the concentration of Ce^{3+}. Localized states in the band gap, resulting from defects, will expand with an increase in Ce^{3+}, which causes a red-shift. The other mechanism is the size effect. The optical band gap will be blue-shifted with a reduction in particle size due to quantum confinement [16,21,24], but the effect of quantum confinement may be ruled out when the size is greater than 10 nm [21]. Chen and Chang [38] have revealed that the red-shift phenomenon for CeO_2 nanoneedles is due to the size effect. In this study, the size of CeO_2 crystallites increases from 10.4 to 66.8 nm when raising calcinations temperature from 673 K to 1273 K. It is seen that the absorption of CeO_2 powders in the UV range had a red-shift effect with raising the calcinations temperature. This phenomenon is due to the quantity of photos reaching the core of a particle depends on the size and the optical properties of CeO_2 crystals. The penetration of light into a particle is influenced by the superficial morphology of the particles, particles formed from larger crystals have a smoother surface than those made from small crystals. On a smooth surface, the incident photons are scattered and mostly lost by reflection have reported by Maris et al. [41]. Moreover, a rough surface allows a greater number of scattered photons to penetrate into the particle [42]. Therefore, based on the above discussion, it is reasonable to conclude that the red-shift of the absorption edge is caused by size effect.

The energy of direct band gap can be determined by fitting the absorption data to the direct transition equation and extrapolating the linear portions of the curves to an absorption of zero [43,44]:

$$\alpha = B_d(h\nu - E_d)^{1/2}/h\nu \quad (4)$$

where E_d is the band gap energy of direct transitions, and B_d is a constant for direct transition.

The dependence of $(\alpha h\nu)^2$ on the band gap energy of CeO_2 nanopowders is shown in Fig. 7(a). From the intersection of the extrapolated linear portion, the E_d values of the CeO_2 nanopowders were determined to be 3.79 eV for dried precursor powder and 3.70, 3.45, and 3.38 eV for the dried precursor powder after calcination for 240 min at 673, 1073, and 1273 K, respectively. These values of E_d are within the range reported in the literature. Maensiri et al. [23] have noted that the correlated direct band gap energies were 3.61, 3.59, and 3.57 eV for CeO_2 samples after calcination at 673, 773, and 873 K, respectively. The E_d values ranged from 3.03 to

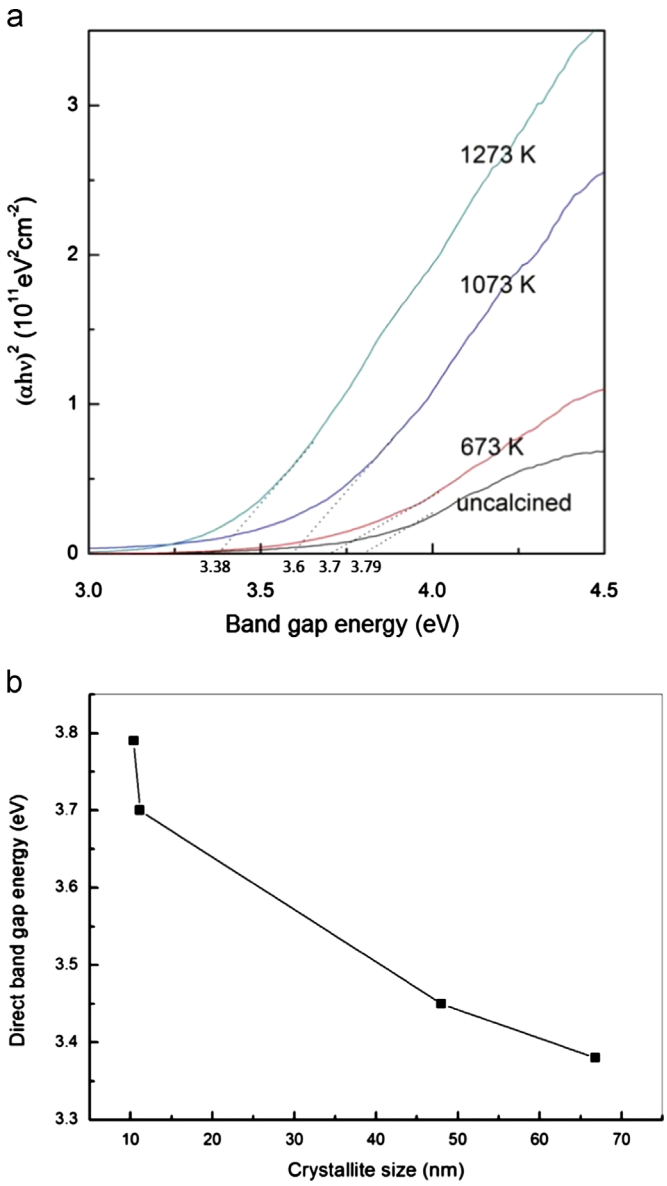

Fig. 7. (a) The relation of $(\alpha h\nu)^2$ and photon energy of CeO_2 nanoparticles for the dried precursor powders after calcination at different temperatures for 240 min, (b) the dependence of the direct band gap energy (E_d) on crystallites size of CeO_2 for the dried precursor powders after calcination at various temperatures for 240 min.

3.08 eV for CeO_2 nanoparticles prepared using a sonochemical process [12]. Ho et al. [45] also reported that the E_d values ranged from 3.36 to 3.62 eV for mesoporous CeO_2 nanostructures prepared via a polyol method. The E_i values of present study corresponded with the values reported by Maensiri et al. [23].

The dependence of E_d on the particle size of dried CeO_2 precursor powders after calcination at various temperatures for 240 min is shown in Fig. 7(b) and reveals that the E_d values decreased from 3.79 to 3.38 eV as the particle size increased from 10.4 nm to 66.8 nm.

Compared to the E_d value of 3.19 eV for the bulk CeO_2 powders determined by UV–vis spectroscopy [35], the crystallite sizes of 10.4 nm, 11.1 nm, 48.0 nm, and 68.8 nm showed an increase in E_g of 0.60, 0.51, 0.26, and 0.19 eV, respectively. Tsunekawa et al. [30] have noted that the E_d values were 3.60, 3.90, and 4.12 eV for nanoparticles with average diameters of 3.2 nm, 2.7 nm, and 2.2 nm, respectively. The results of Tsunekawa et al. [30] also revealed that the E_d values were increased by 0.30 and 0.22 eV when the average diameter decreased from 3.2 nm to 2.7 nm and 2.7 nm to 2.2 nm, respectively. On the other hand, Maensiri et al. [23] also reported that the E_d values were increased by 0.02 eV when the crystal size was decreased from 20 nm to 5 nm, indicating the existence of quantum confinement effects.

The size-related -shift in the band gap of semiconductor nanocrystals can be quantified, which makes the calculation of the particle size from the optical band gap possible [46]. The relation between the effective band gap energy ($E_{g,eff}$) and particle size of a nanoparticle is given as [23,31]:

$$E_{g,eff} = E_{g,b} + \frac{\pi h^2}{2R^2}\left(\frac{1}{m_e^*} + \frac{1}{m_h^*}\right) - \frac{1.8e^2}{\varepsilon R} \quad (5)$$

where $E_{g,b}$ is the bulk band gap energy (3.19 eV), R is the particle radius, m_e^* and m_h^* are the effective masses of the electron and hole, respectively, with $m_e^*=m_h^*=0.4\ m_0$ (m_0 is the mass of a free electron), h is Planck's constant, and ε is the bulk optical dielectric constant.

When the size is comparable to the Bohr radius, where R is very small, the $(1/R^2)$ term becomes dominant and the band gap energy increases with decreasing size (i.e., R). Previous investigations reported quantum size effects in CeO_2 nanostructures [23,24,30,47]. Masui et al. [16] noted that the band gap energies of 4.1 and 2.6 nm CeO_2 nanoparticles prepared via reverse micelles are 3.38 and 3.44 eV, respectively. The band gap energies of 5.8 and 3.6 nm CeO_2 nanoparticles synthesized using sonochemical process are 3.03 and 3.68 eV, respectively, as reported by Yin et al. [47].

However, in the present study, the E_d values increased by 0.09 eV and 0.07 eV when the crystallite size decreased from 11.1 nm to 10.4 nm (673–298 K) and from 66.8 nm to 48.0 nm (1273–1073 K), respectively. The crystallite sizes were in the range of 11.1–68.8 nm in this study. These values are very larger compared to the Bohr radius, causing the $(1/R^2)$ term to approach zero. Therefore, the effect of quantum confinement could be ruled out for sizes larger than 10 nm [21]. However, the results of this study revealed that the E_d values increased by 0.41 eV when the particles have a nonquantum confinement effect (i.e., shape effect) for the present CeO_2 nanocrystallites.

3.3. TEM microstructure of the nano-sized cerium oxide powder

The size and morphology of the dried cerium dioxide precursor powders, analyzed using TEM, are shown in Fig. 8. Fig. 8(a) and (b) shows the bright field (BF) and dark field (DF) images of cerium oxide nanocrystallites with sizes in the range of 6.0–10.0 nm, which is essentially identical to the results calculated from the XRD pattern. Fig. 8(a) and (b) shows that the CeO_2 crystallites prepared using coprecipitation routes are agglomerated, which makes discriminating individual particles

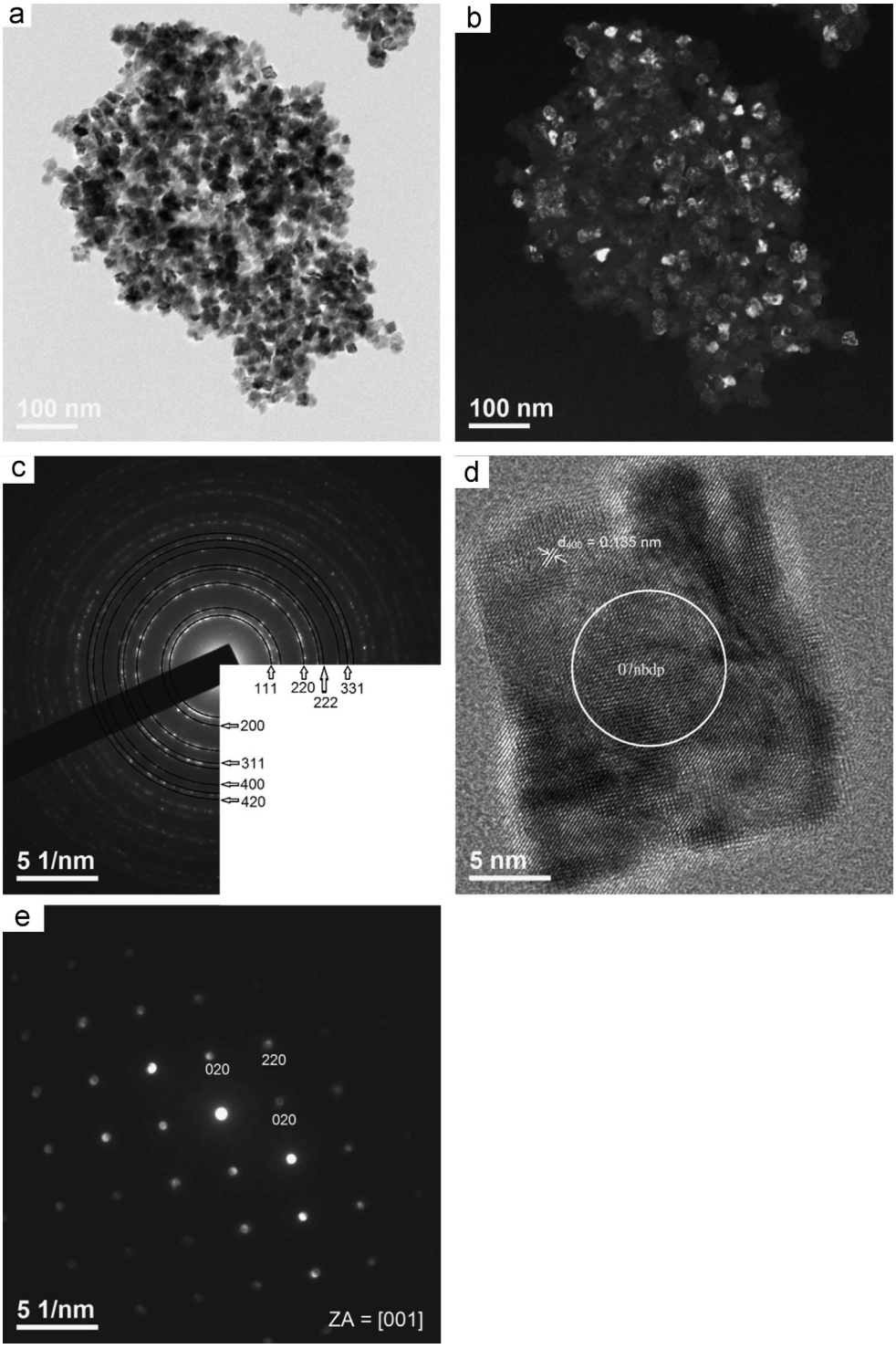

Fig. 8. TEM microstructure and electron diffraction patterns of dried cerium dioxide precursor powders: (a) bright field (BF) image, (b) dark field (DF) image, (c) SAED pattern with indexing corresponding to CeO_2 crystalline, and (d) HRTEM image with a d_{400}-spacing of CeO_2 equal to 0.135 nm, and (e) NBED pattern with indexing corresponding to crystalline CeO_2 with ZA = [001].

difficult. The crystallinity and crystallography of the products were proven using SAED as shown in Fig. 8(c). The SAED measurements show that the particles crystallized with diffraction rings matching the XRD peaks very well. The high-resolution TEM (HRTEM) images of the dried cerium dioxide precursor powders provided further insight into their structure as shown in Fig. 8(d). It indicated that a plate shape and lattice image with a d_{400}-spacing of 0.135 nm. Fig. 8(e) shows the NBED pattern of the site in Fig. 8(d) denoted by a circle (07nbdp). Only a small number of crystallites had been incorporated and crystallized. The NBED pattern indexing corresponds to CeO_2 with a zone axes (ZA) of [001].

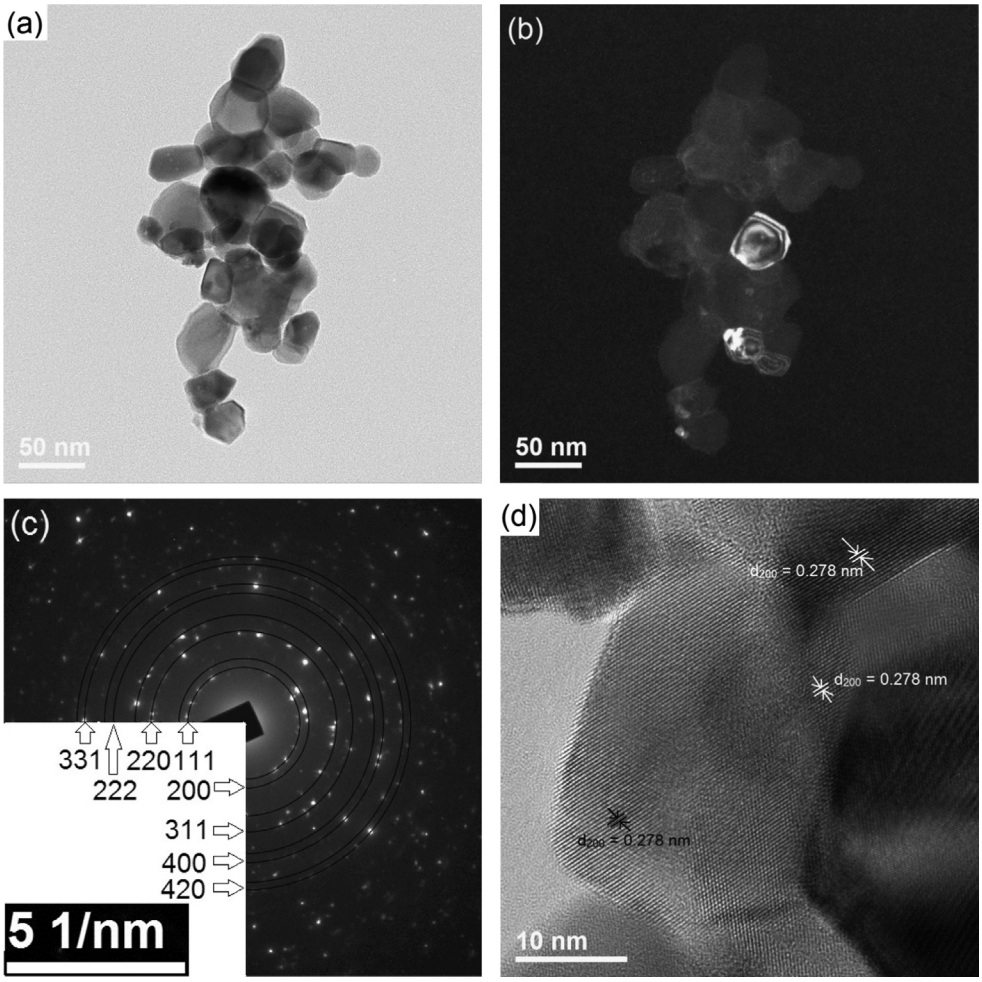

Fig. 9. TEM microstructure of dried CeO_2 precursor powders after calcination at 1073 K for 240 min: (a) BF image, (b) DF image, (c) SAED pattern with indexing corresponding to crystalline CeO_2, and (d) HRTEM image with a d_{111}-spacing of CeO_2 equal to 0.312 nm.

Fig. 9 shows the TEM images, SAED pattern and HRTEM image of cerium dioxide dried precursor powders after calcination at 1073 K for 240 min. Fig. 9(a) and (b) shows the BF and DF images of the calcined products. Although the agglomerated particles were difficult to resolve because of their small size, it was evident that the particles are approximately plate shaped and their size increased before calcination. Some Moiré fringes could be observed in the images, and revealed the presence of crystalline material. Fig. 9(c) shows the SAED pattern of the cerium dioxide precursor powders after calcination at 1073 K for 240 min. The SAED pattern also provides evidence for the formation of crystalline CeO_2. Fig. 9(d) shows the HRTEM image of the CeO_2 particles. It reveals that the calcined product exhibited good crystallinity and clear lattice fringes. The calcined product consisted of 31.6–51.6 nm nanoparticles. The HRTEM image also shows a d_{200}-spacing of 0.278 nm.

4. Conclusions

The growth behavior and optical properties of nanosized cerium oxide (CeO_2) powders were investigated using XRD, TEM, SAED, NBED, HRTEM and UV–vis absorption spectroscopy. The XRD results indicate that dried cerium dioxide precursor powders only contain single phase of CeO_2 before and after calcination. When the dried precursor powders after calcination at various temperatures for 240 min, the crystallite size growth of CeO_2 had a nearly exponential model. The UV–vis absorption spectra revealed that the absorption edge had a small red-shift from 326.7 nm for the dried precursor powders to 390.0 nm for the dried precursor powders after calcination at 1273 K for 240 min. In addition, the indirect band gap energy (E_i) decreased from 3.03 eV to 2.68 eV as the crystallite size increased from 10.4 nm to 66.8 nm, and the direct band gap energy (E_d) also decreased from 3.79 eV to 3.38 eV.

Acknowledgments

The authors gratefully acknowledge the finance support by the National Basic Research Program of China (2009CB939704), Natural Science Foundation of China (No. 51032005) and the Fundamental Research Funds for the Central Universities (Wuhan University of Technology), Mr. LinQing Qin for XRD analysis

(Wuhan University of Technology) and Mr. S.Y. Yao (National Chenh Kung University, Taiwan) for TEM experimentation.

References

[1] N. Izu, W. Shin, N. Murayama, S. Kanzaki, Resistive oxygen gas sensors based on CeO_2 fine powder prepared using mist pyrolysis, Sensors and Actuators B: Chemical 87 (2002) 95–98.

[2] A. Ainirad, M.M.K. Motlagh, A. Maghsoudipoor, A systematic study on the synthesis of Ca, Gd codoped cerium oxide by combustion method, Journal of Alloys and Compounds 509 (2011) 1505–1510.

[3] Y.P. Fu, Y.C. Liu, S.H. Hu, Aqueous tape casting and crystallization behavior of gadolinium-doped ceria, Ceramics International 35 (2009) 3153–3159.

[4] G. Kim, Ceria-promoted three-way catalysts for auto exhaust emission control, Industrial and Engineering Chemistry, Product Research and Development 21 (1982) 267–274.

[5] A. Trovarelli, C. de Leitenburg, M. Boaro, G. Dolcetti, The utilization of ceria in industrial catalysis, Catalysis Today 50 (1999) 353–367.

[6] Y.Z. Li, Q. Sun, M. Kong, W.Q. Shi, J.C. Huang, J.W. Tang, X.J. Zhao, Coupling oxygen ion conduction to photocatalysis in mesoporous nanorod-like ceria significantly improves photocatalytic efficiently, Journal of Physical Chemistry C 115 (2011) 14050–14057.

[7] C.R. Stanek, A.H.H. Tan, R.W. Grimes, S.L. Owens, Atomistic simulation of CeO_2 surface hydroxylation: implications for glass polishing, Journal of Materials Science 43 (2008) 4157–4162.

[8] S. Tsunekawa, R. Sahara, Y. Kawazoe, A. Kasuya, Origin of the blue-shift in ultraviolet absorption spectra of nanocrystalline CeO_2 particles, Materials Transactions JIM 41 (2000) 1104–1107.

[9] R.P. Netterfield, W.G. Sainty, P.J. Martin, S.H. Sie, Properties of CeO_2 thin films prepared by oxygen-ion-assisted deposition, Applied Optics 24 (1985) 2267–2272.

[10] R.P. Andres, R.S. Aveback, W.L. Brown, L.E. Brus, W.A. Goddard III, A. Kaldor, S.G. Louie, M. Moscovits, P.S. Peercy, S.J. Riley, R. W. Siegel, F. Spaepen, Y. Wang, Research opportunities on clusters and cluster-assembled materials, Journal of Materials Research 4 (1989) 704–736.

[11] M. Taguchi, S. Takami, T. Adschiri, T. Nakane, K. Sato, T. Naka, Supercritical hydrothermal synthesis of hydrophilic polymer-modified water-dispersible CeO_2 nanoparticles, CrystEngComm 13 (2011) 2841–2848.

[12] S.K. Sahoo, M. Mohapatra, A.K. Singh, S. Anand, Hydrothermal synthesis of single crystalline nano CeO_2 and its structural, optical and electronic characterization, Materials and Manufacturing Processes 25 (2001) 982–989.

[13] S. Pavasupreea, Y. Suzukia, S. Pivsa-Artb, S. Yoshikawaa, Preparation and characterization of mesoporous MO_2 (M: Ti, Ce, Zr, and Hf) nanopowders by a modified sol-gel method, Ceramics International 31 (2005) 959–963.

[14] H. Yang, C. Huang, A. Tang, X. Zhang, W. Yang, Microwave-assisted synthesis of ceria nanoparticles, Materials Research Bulletin 40 (2005) 1690–1695.

[15] Z. Zhang, X. Ju, Z.Y. Wu, T. Liu, T.D. Hu, N.Y. Xie, Structural characteristics of cerium oxide nanocrystals prepared by the microemulsion method, Chemistry of Materials 13 (2001) 4192–4197.

[16] T. Masui, K. Fujiwara, K. Machida, G. Adachi, Characterization of cerium (IV) oxide ultrafine particles prepared using reversed micelles, Chemistry of Materials 9 (1997) 2197–2204.

[17] D.S. Zhang, J.P. Zhang, L.Y. Shi, Facile synthesis of ceria rhombic microplates, Journal of Materials Science 43 (2008) 5647–5650.

[18] S.A. Hassanzadeh-Tabrizi, M. Mazaheri, M. Aminzare, S.K. Sadmezhaad, Reverse precipitation synthesis and characterization of CeO_2 nanopowder, Journal of Alloys and Compounds 497 (2010) 499–502.

[19] G.L. Yang, H.H. Ko, Y.W. Hsu, K.H. Yang, M.C. Wang, J.J. Han, X. J. Zhao, Growth behavior of nanosized ceria powders prepared by coprecipitation routes, Ceramics International 39 (2013) 6805–6811.

[20] B. Liu, Q.J. Li, X.B. Du, B.B. Liu, M.G. Yao, Z.P. Li, R. Liu, D.D. Liu, X. Zou, H. Lv, D.M. Li, B. Zou, T. Cui, G.T. Zou, Facile hydrothermal synthesis of CeO_2 nanosheets with high reactive exposure surface, Journal of Alloys and Compounds 509 (2011) 6720–6724.

[21] X.H. Lu, X. Huang, S.L. Xie, D.Z. Zheng, Z.Q. Liu, C.L. Liang, Y. X. Tong, Facile electrochemical synthesis of single crystalline CeO_2 octahedrons and their optical properties, Langmuir 26 (2010) 7569–7573.

[22] B.D. Cullity, S.R. Stock, Elements of X-Ray Diffraction, second ed., Addison-Wesley, Reading, MA87.

[23] S. Maensiri, C. Masingboon, P. Laokul, W. Jareonboon, V. Promarak, P. L. Anderson, S. Seraphin, Egg white synthesis and photoluminescence of platelike clusters of CeO_2 nanoparticles, Crystal Growth and Design 7 (2007) 950–955.

[24] Z.X. Li, L.L. Li, Q. Yuan, W. Feng, J. Xu, L.D. Sun, W.G. Song, C. H. Yan, Sustainable and facile route to nearly nanodisperse spherical aggregates of CeO_2 nanocrystals with ionic liquids and their catalytic activities for Co oxidation, Journal of Physical Chemistry C 112 (2008) 18405–18411.

[25] M. Taguchi, S. Takami, T. Naka, T. Adschiri, Growth mechanism and surface chemical characteristics of dicarboxylic acid-modified CeO_2 nanocrystals produced in supercritical water: tailor-made-water-soluble CeO_2 nanocrystals, Crystal Growth and Design 9 (2009) 5297–5303.

[26] H.S. Liu, T.S. Chin, S.Y. Chiu, K.H. Chung, C.S. Chung, M.T. Liu, Hydroxyapatite synthesized by a simplified hydrothermal method, Ceramics International 23 (1997) 19–25.

[27] C.W. Kuo, Y.H. Shen, S.B. Wen, H.E. Lee, I.M. Hung, H.H. Huang, M.C. Wang, Phase transformation kinetics of 3 mol% yttria partially stabilized zirconia (3Y-PSZ) nanopowders prepared by a non-isothermal process, Ceramics International 37 (2011) 341–347.

[28] J.G. Li, T. Ikegami, J.H. Lee, T. Mori, Characterization and sintering of nan9crystalline CeO_2 powders synthesized by a mimic alkoxide method, Acta Materialia 49 (2001) 419–426.

[29] J.K.L. Lai, C.H. Shek, G.M. Lin, Grain growth kinetics of nanocrystalline SnO_2 for long-term isothermal annealing, Scripta Materialia 49 (2003) 441–446.

[30] S. Tsunekawa, T. Fukuda, A. Kasuya, Blue-shift in ultraviolet absorption spectra of monodisperse CeO_{2-x} nanoparticles, Journal of Applied Physics 87 (2000) 1318–1321.

[31] E.K. Goharshadi, S. Samiee, P. Nancarrow, Fabrication of cerium oxide nanoparticles: characterization and optical properties, Journal of Colloid and Interface Science 356 (2011) 473–480.

[32] J.F. de Lima, R.F. Martins, C.R. Neri, O.A. Serra, ZnO:CeO_2-based nanopowders with low catalytic activity as UV absorbers, Applied Surface Science 255 (2009) 9006–9009.

[33] A.P. Popov, A.V. Priezzhev, J. Lademann, R. Myllylä, TiO_2 nanoparticles as an effective UV-B radiation skin-protective compound in sunscreens, Journal of Physics D: Applied Physics 38 (2005) 2564–2570.

[34] R.A. Van Leeuwen, C.J. Hung, D.R. Kammler, J.A. Switzer, Optical and electronic transport properties of electrodeposited thallium(III) oxide films, Journal of Physical Chemistry 99 (1995) 15247–15252.

[35] Z.Z. Orel, B. Orel, Optical properties of pure CeO_2 and mixed CeO_2/SnO_2 thin film coatings, Physica Status Solidi B 181 (1994) K33–K36.

[36] M.Y. Chen, X.T. Zu, X. Xiang, H.L. Zhang, Effects of ion irradiation and annealing on optical and structural properties of CeO_2 films on sapphire, Physica B 389 (2007) 263–268.

[37] C. Sun, H. Li, H. Zhang, Z. Wang, L. Chen, Controlled synthesis of CeO_2 nanorods by a solvothermal method, Nanotechnology 16 (2005) 1454–1463.

[38] H.I. Chen, H.Y. Chang, Synthesis and characterization of nanocrystalline cerium oxide powders by two-stage non-isothermal precipitation, Solid State Communications 133 (2005) 593–598.

[39] F.H. Scholes, A.E. Hughes, S.G. Hardin, P. Lynch, P.R. Miller, Influence of hydrogen peroxide in the preparation of nanocrystalline ceria, Chemistry of Materials 19 (2007) 2321–2328.

[40] P. Patsalas, S. Logothetidis, C. Metaxa, Optical performance of nanocrystalline transparent ceria films, Applied Physics Letters 81 (2002) 466–468.

[41] A.J. Maria, K.L. Yeung, C.Y. Lee, P.L. Yue, C.K. Chan, Size effect in gas-phase photo-oxidation of trichloroethylene using nanometer-sized TiO_2 catalyst, Journal of Catalysis 192 (2000) 185–196.

[42] Q.Z. Yan, X.T. Su, Z.Y. Huang, C.C. Ge, Sol-gel auto-igniting synthesis and structural property of cerium-doped titanium dioxide nanosized powders, Journal of the European Ceramic Society 26 (2006) 915–921.
[43] E. Ziegler, A. Heinrich, H. Oppermann, G. Stover, Electrical properties and non-stoichiometry in ZnO single crystals, Physica Status Solid A 66 (1981) 635–648.
[44] S. Hingorani, V. Pillai, P. Kumar, M.S. Multani, D.O. Shah, Microemulsion mediated synthesis of zinc-oxide nanoparticles for varistor studies, Materials Research Bulletin 28 (1993) 1303–1310.
[45] C. Ho, J.C. Yu, T. Kwong, A.C. Mak, S. Lai, Morphology-controllable synthesis of mesoporous CeO_2 nano- and microstructures, Chemistry of Materials 17 (2005) 4514–4522.
[46] Y. Dieckmann, H. Colfen, H. Hofmann, A. Petri-Fink, Particle size distribution measurements of manganese-doped ZnS nanoparticles, Analytical Chemistry 81 (2009) 3889–3895.
[47] L. Yin, Y. Wang, G. Pang, Y. Koltypin, A. Gedanken, Sonochemical synthesis of cerium oxide nanoparticles-effect of additives and quantum size effect, Journal of Colloid and Interface Science 246 (2002) 78–84.